Available online at www.sciencedirect.com
ScienceDirect
Infrared Physics & Technology xxx (2006) xxx–xxx
INFRARED PHYSICS & TECHNOLOGY
www.elsevier.com/locate/infrared

Si doped GaAs/AlGaAs terahertz detector and phonon effect on the responsivity

A.B. Weerasekara [a], M.B.M. Rinzan [a], S.G. Matsik [a], A.G.U. Perera [a,*], M. Buchanan [b], H.C. Liu [b], G. von Winckel [c], A. Stintz [c], S. Krishna [c]

[a] Department of Physics and Astronomy, Georgia State University, Atlanta, GA 30303, USA
[b] Institute for Microstructural Sciences, National Research Council, Ottawa, Ont., Canada K1A 0R6
[c] Center for High Technology Materials, EECE Dept., University of New Mexico, Albuquerque, NM 87106, USA

Abstract

Terahertz detection capability of an n-type heterojunction interfacial work function internal photoemission (HEIWIP) detector is demonstrated. Threshold frequency, f_0, of 3.2 THz (93 μm) was obtained by using n-type GaAs emitter doped to 1×10^{18} cm^{-3} and $Al_{0.04}Ga_{0.96}As$ single barrier structure. The detector shows a broad spectral response from 30 to 3.2 THz (10–93 μm) with peak responsivity of 6.5 A/W at 7.1 THz under a forward bias field of 0.7 kV/cm at 6 K. The peak quantum efficiency and peak detectivity are ~19% and $\sim 5.5 \times 10^8$ Jones, respectively under a bias field of 0.7 kV/cm at 6 K. In addition, the detector can be operated up to 25 K.

PACS: 85.60.Gz; 78.66.Fd; 78.67.Pt

1. Introduction

In recent years, terahertz detectors (0.1–30 THz) have been the center of attraction in many areas such as medical diagnostic, security, astronomy, communication, etc. Numerous advantages can be achieved upon the availability of a well developed terahertz detector. Bolometers and pyroelectric detectors are currently the most popular detectors in the THz region. However, a main drawback of these detectors is the slow photoresponse which hinders development of many promising THz applications. In addition, the difficulty of integrating these detectors into focal plane array for terahertz imaging. Therefore, photon detectors which possess faster photoresponse and focal plane array capability, are good candidates for THz applications.

In HEIWIP detectors, an undoped alloy semiconductor material is used as the barrier and highly doped semiconductor as the emitter. The internal work function, Δ, is defined from the top of the Fermi energy in the emitter to the bottom of the conduction band of the barrier. The Internal work function is given by $\Delta = \Delta_x + \Delta_d$, and $\Delta_d = \Delta_{\text{narr}} - E_F$, where Δ_x is the conduction band offset between the emitter and the barrier due to composition, Δ_{narr} is the band gap narrowing in the emitter layer due to doping, and E_F is the Fermi energy. The zero response threshold f_0 is determined by the energy difference from the Fermi level in the emitter to the bottom of the conduction band of the barrier. The threshold frequency of the detector, f_0, can be tailored by changing the alloy fraction, x [1,2]. Threshold frequency, f_0, is given by $f_0 = \Delta/4.133$ in terahertz. Here Δ is in meV.

The reported results on HEIWIP detectors are limited to p-type structures [3,4]. p-type HEIWIP detectors have shown the ability to push the threshold limit beyond 5 THz (>60 μm). Tailorability of threshold frequency f_0 with different Al fractions in p-type HEIWIP terahertz detectors has been shown for three detectors with $f_0 = 4.6$, 3.6, and 3.2 THz [2]. The Al fraction used for the 3.2 THz threshold detector is 0.005. This 0.005 Al fraction is close to the practical lowest limit for MBE growth.

* Corresponding author. Tel.: +1 404 6512279; fax: +1 404 6511427.
E-mail address: uperera@gsu.edu (A.G.U. Perera).

1350-4495/$ - see front matter © 2006 Elsevier B.V. All rights reserved.
doi:10.1016/j.infrared.2006.10.019

Therefore, lowering the work function further may not be possible. One alternative to this is to use an inverted HEIWIP structure [4]. In the inverted structure, p-doped $Al_xGa_{1-x}As$ is used as the emitters and undoped GaAs is used as the barriers. Therefore, smaller work function can be designed by increasing the Al fraction and thereby a lower threshold frequency can be achieved. However, the reported lowest threshold obtained with inverted structure is 2.3 THz (128 μm). The other alternative is to use an n-type HEIWIP detectors. For the same small Al fraction composition, the work function in n-type HEIWIP is smaller than the that of p-type HEIWIP because of the smaller effective mass of electrons compared to the effective mass of holes. According to initial theoretical calculations, it is possible to achieve the threshold frequency below 3 THz in n-type HEIWIP with relatively larger Al fraction. For an example, theoretically, 1 THz threshold frequency can be obtained in n-type HEIWIP with Al fraction of 0.03. In this paper, the capability of extending the zero response threshold to 3 THz limit by using n-type single barrier HEIWIP is demonstrated.

2. Device design

The device structure as shown in Fig. 1(a) consists of an undoped 1 μm thick $Al_xGa_{1-x}As$ ($x = 0.04$) barrier layer sandwiched between two n-doped (Si) 1×10^{18} cm^{-3} GaAs contact layers with the top contact being 100 nm and the bottom contact being 700 nm in thickness. GaAs doped to 5×10^{18} cm^{-3} with Si was used as the substrate. The top and the bottom contact layers work as emitters for reverse and forward bias operations. The Si doping concentration and the Al fraction were verified by secondary ion mass spectrometry (SIMS) and are shown in Fig. 1(b). The thickness of the top contact layer was to kept to 100 nm to allow a substantial amount of light to pass through to the bottom contact. NiGeAu was deposited on bottom and top layers as ring ohmic contacts. Note that the highly doped substrate is electrically isolated from the active layers. The conduction band diagram of the structure is shown in Fig. 1(a). The calculated Fermi energy in the emitter layers, E_F is 56 meV while the conduction band discontinuity in the GaAs/AlGaAs interface is 32 meV for $x = 0.04$. Considering band gap narrowing [5] of 35–45 meV in the GaAs emitter layer due to 1×10^{18} cm^{-3} n doping, the calculated work function is between 10 and 20 meV, which corresponds to 2.4–5.0 THz (125–60 μm) cutoff frequency. The work function was estimated to be 13–14 meV according to Arrhenius analysis.

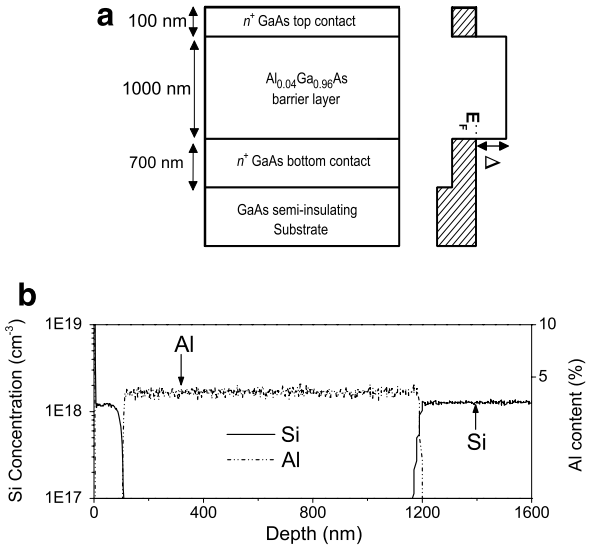

Fig. 1. (a) Single barrier n-type HEIWIP structure. Top and bottom contact layers (emitters) are n-doped to 1×10^{18} cm^{-3} and the substrate is n-doped to 5×10^{18} cm^{-3}. In addition, the top and the bottom contact layers work as emitters also. The conduction band diagram of the structure is also shown. (b) Secondary ion mass spectroscopy (SIMS) data are given for aluminum content and silicon concentration in the structure. Aluminum content is 4% in the barrier and silicon concentration is $\sim 1 \times 10^{18}$ cm^{-3}.

3. Device characterization

Low temperature dark current–voltage measurements were performed on the device from 4.2 to 120 K. Fig. 2 shows dark current density–voltage behavior for temperatures ranging from 10 to 40 K. The dark current increases rapidly after 1.5 kV/cm in forward bias and −1.0 kV/cm in the reverse bias. Therefore, the device performance is restricted in this bias field region. Spectral measurements were performed by using a fast Fourier transform infrared spectrometer (FTIR). A silicon composite bolometer was used to calibrate the raw spectra obtained with the device. Responsivity was calculated by using $R = \frac{R_{raw}}{R_{bol}} \frac{SG}{R_{\|}}$. Here R_{raw} and R_{bol} are the detector raw spectral response and the bolometer spectral response respectively, S is the voltage sensitivity of the bolometer, G is the geometrical area correction factor, and $R_{\|}$ is the parallel resistance of the device and the load resistor. Responsivity for different bias field strengths is shown in Fig. 3 at 6 K. The maximum peak

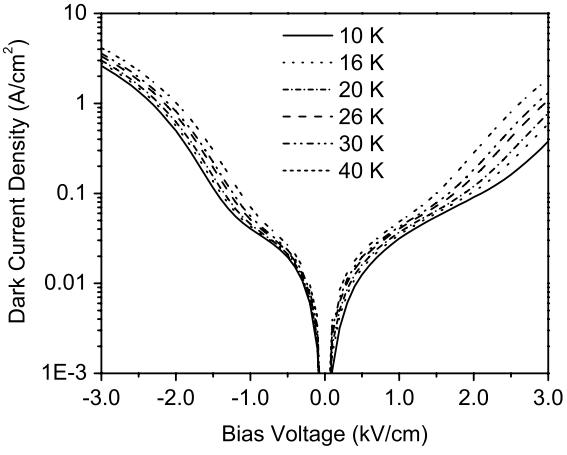

Fig. 2. The dark current density change with applied bias field is shown for different temperatures. The detector can be operated from −1.0 to 1.5 kV.cm since the dark current density is relatively low in this region.

Please cite this article in press as: A.B. Weerasekara et al., Si doped GaAs/AlGaAs terahertz detector and phonon effect ..., Infrared Phys. Techn. (2006), doi:10.1016/j.infrared.2006.10.019

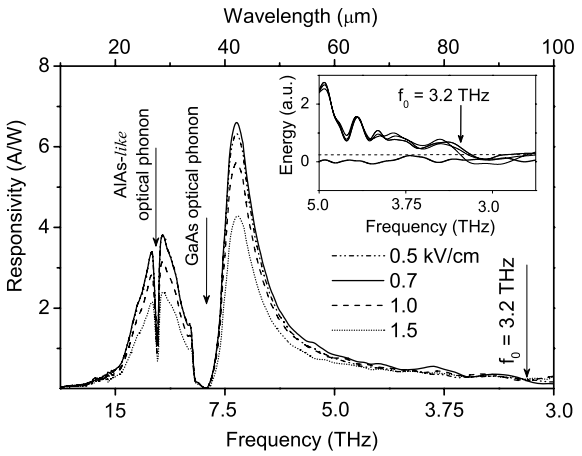

Fig. 3. Responsivity variation with applied bias field in forward bias (photoemission from bottom contact) is shown. The highest responsivity is 6.5 A/W at 0.7 kV/cm at 6 K. The threshold frequency is 3.2 THz. The threshold frequency was determined by the instrument noise level. The several spectral curves at 0.7 kV/cm are shown in the inset. The dotted line represents the maximum noise level.

response of 6.5 A/W at 7.1 THz (42 μm) was obtained at 0.7 kV/cm bias field. A strong light reflection occurs around 11 THz (27 μm) and 8.3 THz (36 μm) due to the AlAs-like and GaAs optical phonons, giving two minima around 11 THz (27 μm) and 8.3 THz (36 μm) in the responsivity spectra. The zero response threshold was estimated by considering the instrument noise level as shown in the inset to Fig. 3. The zero response threshold was found to be 3.2 THz (93 μm). The lowest threshold frequency reported for any type of HEIWIP detector is 2.3 THz (128 μm) [4]. It is noteworthy that the response of the single barrier detector reported here matches the p-type multi-emitter detector reported in Ref. [4]. The peak responsivity (R_{peak}), the peak quantum efficiency (η_{peak}), and the peak detectivity (D^*_{peak}) at 7.1 and 10.4 THz for different bias fields are given in Table 1. The peak quantum efficiency is about 19% at 0.7 kV/cm. The detectivity was calculated by using the shot noise. The device can be operated under reverse bias and peak responsivities of 1.7, 1.1, and 0.7 A/W at 10 THz (30 μm) were observed at −0.25, −0.5, and −0.75 kV/cm bias fields, respectively. The peak responsivity under 0.7 kV/cm bias field drops from 6.5 A/W to 0.1 A/W when the operating temperature changes from 6 K to 25 K.

Table 1
The responsivity (R_{peak}), the quantum efficiency (η_{peak}), and the detectivity (D^*_{peak}) at 7.1 and 10.4 THz frequencies for different bias fields

Bias Field (kV/cm)	Peak at 7.1 THz			Peak at 10.4 THz		
	R_{peak} (A/W)	η_{peak} (%)	D^*_{peak} (×10^8 Jones)	R_{peak} (A/W)	η_{peak} (%)	D^*_{peak} (×10^8 Jones)
0.2	3.0	8.9	5.5	2.1	9.1	3.8
0.5	6.1	18.2	6.4	3.7	16.4	3.8
0.7	6.5	18.9	5.5	3.7	16.4	3.1
1.0	5.5	16.5	3.4	3.1	13.5	2.1
1.5	4.1	12.3	2.1	2.4	10.3	1.2

4. Forward and reverse bias photoresponses

The device photoresponses in the forward and the reverse bias operations are shown in Fig. 4(a). When the device is in forward bias, the photoresponse is from the bottom contact layer, whereas, the photoresponse is from the top contact layer when the device is in reverse bias. The responsivity from the bottom contact layer is much higher than that of the top contact layer. The peak responsivity of the top contact layer is ~1.2 A/W while it is 6.5 A/W for the bottom contact layer. The reason for this large difference is the higher photoabsorption in the bottom contact layer since bottom contact layer is much thicker than the top contact layer. The highest photoresponse efficiency in the top contact layer occurs around 30 THz while the highest photoresponse efficiency in the bottom contact layer occurs at 7.1 THz. It is not expected for the two shapes of the responsivities from bottom and top contact layer to be different as the device design is almost symmetric. Specially, the doping concentrations are same in the top and bottom contact layers as shown in the SIMS results (Fig. 1(b)). When the two responsivities are normalized (see Fig. 4(b)), a clear difference between the two responsivity spectra can be seen. The photoresponse efficiency from the bottom contact layer is considerably smaller than that of the top contact layer in the spectral range above 8 THz. In order to understand the physics behind

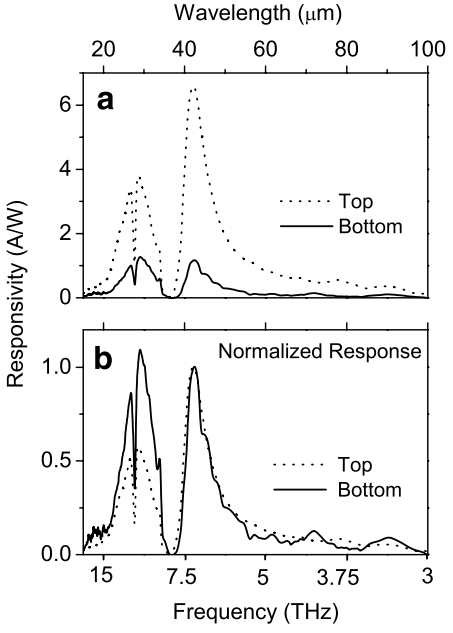

Fig. 4. (a) Experimental forward and reveres bias responses. Peak responsivity of 6.5 A/W for forward bias is at 7.1 THz (Bottom contact layer – dotted line) while 1.2 A/W for reversed bias is at 10 THz (Top contact layer – solid line). (b) Forward and reverse bias spectra normalized to the peak value at 7.1 THz.

Please cite this article in press as: A.B. Weerasekara et al., Si doped GaAs/AlGaAs terahertz detector and phonon effect ..., Infrared Phys. Techn. (2006), doi:10.1016/j.infrared.2006.10.019

this, responsivity modeling was carried out. The photoresponse of HEIWIP detectors mainly depends on two processes. The first one is photoabsorption efficiency in the emitter layer and the second one is photoexcited carrier emission over the barrier [6]. Free carrier absorption efficiency in the emitter (in this case top and bottom contacts) can be calculated by

$$\eta_a = 2I_{ave}\frac{\omega}{c}\mathrm{Im}[\varepsilon(\omega)]W, \tag{1}$$

where $\mathrm{Im}[\varepsilon(\omega)]$ is the imaginary part of the dielectric function of the emitter layer, I_{ave} is the average light intensity in the emitter, and W is thickness of the emitter. The dielectric function is given by

$$\varepsilon(\omega) = \varepsilon_\infty\left(1 - \frac{\omega_p^2}{\omega^2 + i\omega\gamma}\right) + \sum_{j=1}^{n}\frac{S_j\omega_j^2}{\omega_j^2 - \omega^2 - i\Gamma_j\omega}, \tag{2}$$

where ε_∞, ω_p, and ω_j are the high frequency dielectric constant, the plasma frequency, and the optical phonon frequencies, respectively. S, Γ_j, and γ are the optical phonon strengths, the optical phonon broadening constant, and the plasma oscillator damping constant, respectively.

The calculated free carrier absorption is shown in Fig. 5 for both the top and the bottom contact layers. As expected, both shapes are the same. The highest absorption occurs at 7.6 THz (40 μm) in both the top and the bottom contact layers. The bottom contact layer absorption is higher than that of the top contact layer because the thickness of the bottom contact layer is larger. The photoemission efficiency over the barrier can be calculated by using the escape cone model [7] and the hot carrier transport mechanism [8,6]. In the photoemission calculations, energy independence of scattering lengths was assumed. The energy loss from electron–phonon collision was also ignored. The total quantum efficiency η can be calculated by combining the photoabsorption efficiency and the photoemission efficiency [1]. Finally, the responsivity can be calculated by using

$$R = \frac{q\eta\lambda}{hc}, \tag{3}$$

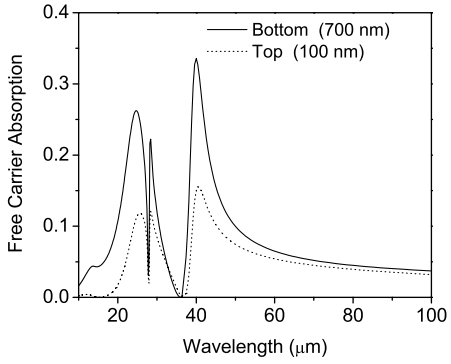

Fig. 5. The calculated free carrier absorption probability in the top and the bottom contact layers for the structure. Highest absorption occurs at 40 μm in both layers.

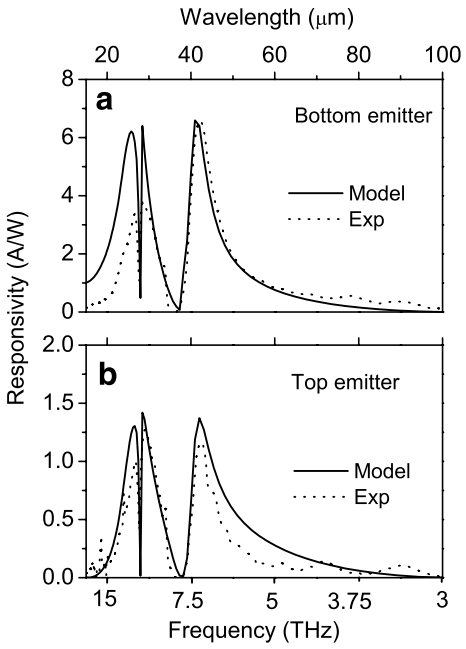

Fig. 6. Model calculation and experimental photoresponse: (a) Forward bias (emission from the bottom contact); (b) reverse bias (emission from the top contact). Model calculation fits the experimental spectra of the top contact layer. Responsivity in the forward bias (emission from bottom emitter) is less than the model in the higher frequency region (>8 THz).

where q is the unit charge, η is total quantum efficiency, λ is wavelength, h is the Planck constant and c is the speed of light. The calculated responsivities for the top contact layer and the bottom contact layer are shown in Fig. 6. While the model and experimental responsivity agrees well for the top contact layer as shown in Fig. 6(b), the experimental responsivity for the bottom contact layer does not fit in the model responsivity as seen in Fig. 6(a). A better agreement is found only in the frequency region below 10 THz (30 μm). However, the experimental responsivity in the higher frequency region (>10 THz) is much smaller than the model responsivity. This low photoresponse efficiency region lies above the GaAs optical phonon. Therefore, the reason for the lower photoresponse than expected may be due to a phonon emission by photoexcited electrons. Since the thickness of the top contact layer is much smaller, the effect of the phonon emission on the reverse bias responsivity should be minimum.

When compared with p-type HEIWIP detectors, the noticeable difference is the high Al fraction for the same threshold frequency and the positions of the maximum peak in n-type HEIWIP detectors. Recently, p-type terahertz detectors with cutoff frequencies of 3.2, 3.6, and 4.6 THz were reported [2] for different Al fractions. Al fraction of 0.005, which is around the lowest limit for MBE, was used to obtain 3.2 THz threshold in the p-type detector while the same threshold frequency can be obtained with Al fraction of 0.04 in the n-type detectors as shown in this study. Furthermore, the highest responsivity is around 10 THz.

Please cite this article in press as: A.B. Weerasekara et al., Si doped GaAs/AlGaAs terahertz detector and phonon effect ..., Infrared Phys. Techn. (2006), doi:10.1016/j.infrared.2006.10.019

5. Conclusion

Extending the threshold frequency below 3 THz in photon detectors is possible. Threshold extending below 3 THz has been achieved in HEIWIP whereas it is inherently difficult in QWIP and Schottky barrier photo detectors. The lowest threshold limit obtained in HEIWIP (not for the inverted structure) is 3.2 THz [2] and the Al fraction in the barrier region is 0.005. This 0.005 Al fraction is close to the lowest practical limit that can be achieved for any present growth technology. Therefore, this hinders the extension the threshold limit beyond 3 THz in p-type GaAs/$Al_xGa_{1-x}As$ HEIWIP detectors. One alternative to this is n-type $Al_xGa_{1-x}As$/GaAs detectors. Smaller work function can be designed with relatively higher Al fraction compared to p-type HEIWIP detector. In this study, threshold frequency of 3.2 THz was obtained with much higher Al fraction, $x = 0.04$ when compared to 0.005 in p-type HEIWIP detector [2]. Therefore, extending threshold even beyond 3 THz can be easily achieved with n-type HEIWIP detector.

Acknowledgement

This work was supported in part by the US NSF under grant No. ECS-0553051.

References

[1] D.G. Esaev, M.B.M. Rinzan, S.G. Matsik, A.G.U. Perera, J. Appl. Phys. 96 (2004) 4588.
[2] S.G. Matsik, M.B.M. Rinzan, A.G.U. Perera, H.C. Liu, Z.R. Wasilewski, M. Buchanan, Appl. Phys. Lett. 82 (2003) 139.
[3] M.B.M. Rinzan, A.G.U. Perera, S.G. Matsik, H.C. Liu, M. Buchanan, G. von Winckel, A. Stintz, S. Krishna, Infrared Phys. Technol. 47 (2005) 188.
[4] M.B.M. Rinzan, A.G.U. Perera, S.G. Matsik, H.C. Liu, Z.R. Wasilewski, M. Buchanan, Appl. Phys. Lett. 86 (2005) 071112.
[5] Huade Yao, A. Compaan, Appl. Phys. Lett. 57 (1990) 147.
[6] A.G.U. Perera, H.X. Yuan, M.H. Francombe, J. Appl. Phys. 77 (1995) 915.
[7] R. Williams, in: R.K. Willardson, A.C. Beer (Eds.), Semiconductors and Semimetals, vol. 6, Academic Press, 1970.
[8] J.M. Mooney, J. Silverman, IEEE Trans. Electron Dev. 32 (1985) 33.

Please cite this article in press as: A.B. Weerasekara et al., Si doped GaAs/AlGaAs terahertz detector and phonon effect ..., Infrared Phys. Techn. (2006), doi:10.1016/j.infrared.2006.10.019